Highly Selective and Stable Isolated Non-Noble Metal Atom Catalysts for Selective Hydrogenation of Acetylene

Baoai Fu,[1] Alan J. McCue,[2] Yanan Liu,[1,*] Shaoxia Weng,[1] Yuanfei Song,[1] Yufei He,[1] Junting Feng[1] and Dianqing Li[1,*]

[1]*State Key Laboratory of Chemical Resource Engineering, Beijing Engineering Center for Hierarchical Catalysts, Beijing University of Chemical Technology, Beijing, 100029, China*

[2]*Department of Chemistry, University of Aberdeen, Aberdeen AB24 3UE, U.K.*

* Corresponding author

Address: Box 98, 15 Bei San Huan East Road, Beijing 100029, China

Tel: +86 10 64436992 Fax: +86 10 64436992

E-mail address: ynliu@mail.buct.edu.cn (Yanan Liu); lidq@mail.buct.edu.cn (Dianqing Li)

ABSTRACT

A strategy to fabricate a stable and site-isolated Ni catalyst is reported. Specifically, Mo_3S_4 clusters allowed individual Ni atoms to bond with Mo and S to create a type of active site. Site-isolated Ni_1MoS/Al_2O_3 sample exhibited high performance in the selective hydrogenation of acetylene. Specifically, 90% ethylene selectivity was achievable at full acetylene conversion under relatively mild reaction conditions without any obvious decay in performance observed during longer testing periods. In contrast, a reference catalyst with Ni ensembles exhibited poor selectivity and stability. DFT calculations suggested H_2 molecules were activated by a heterolytic route over Ni_1MoS/Al_2O_3 which enhanced reaction rate. Improved selectivity originated from the unique isolated $Ni^{\delta+}$ structure induced by Mo and S which facilitated product desorption as opposed to over-hydrogenation or oligomerization. This work provides a feasible way to construct site-isolated catalysts with higher active metal loadings and opens up an opportunity in selective hydrogenation.

Keywords: Non-noble Ni catalysts; Isolated $Ni^{\delta+}$ structure; Selective hydrogenation; Mo_3S_4 cluster; Confinement strategy

1. Introduction

Global targets of sustainable development in the energy and environmental fields have seen site isolated catalysts receive widespread attention due to their maximal atom utilization and special catalytic behavior,[1, 2] which is associated with low coordination number[3], quantum confinement of metal atoms[4] and/or strong interactions with the catalyst support[5]. Traditional fabrication strategies for single atom catalysts are highly dependent upon the initial adsorption/binding of a metal precursor with a support and often require lower metal loading to be effective.[6] However, challenges still emerge from the heterogeneity of such a system (namely, the metal atoms can locate at different support sites).[7] Also, owing to high surface free energy, individual metal atoms are generally mobile on the support surface and thus aggregate, especially in reaction processes occurring at elevated temperatures.[8] As a consequence of these points, the development of alternative fabrication strategies to prepare well-defined and stable site-isolated catalysts with higher metal loading are very desirable, albeit challenging.

The term 'metal cluster' refers to a structure in which three or more metal atoms are directly bonded to each other to form metal-metal bonds (abbreviated as M-M), while a 'sulfur-containing metal cluster' occurs when one or more metal atom is replaced by S atom.[9, 10] Sulfur-containing metal clusters like M_3S_4 (M = Mo or W) with a cubane structure have been touted as an ideal platform for the preparation of highly dispersed catalysts owing to their ultra-high specific surface area and uniformity.[11] Recent literature[12] indicates that a second metal such as cobalt or nickel can be introduced into the Mo_3S_4 structure, which itself, provides a platform for constructing site-isolated catalysts. However, whether the Co/Ni atoms act as discrete active sites or as a promoter for the underlying Mo_3S_4 cluster remains unclear. It would therefore be highly desirable to gain greater insight into the properties of these clusters from an experimental perspective.

The selective hydrogenation of alkyne impurities in alkene rich streams is an important industrial process for purifying alkenes produced from petroleum cracking.[13,14] The critical requirements for this process are (i) to achieve high selectivity

to the alkene, especially at high alkyne conversion;[15] (ii) to minimize hydrogenation of any alkene produced (or present in inlet stream) especially at high alkyne conversion;[16] and (iii) to achieve high durability against deactivation via carbonaceous deposits associated with oligomerization.[17] Whilst Pd-based catalysts are often used for alkyne hydrogenation, non-noble Ni-based catalysts could also be used due to their good hydrogenation activity and lower cost/higher abundance. However, Ni catalysts are generally less selective at high conversion for this type of process.[18] In recent years, much focus has been paid to the development of efficient and selective Ni-based catalysts by introducing a second element to fabricate an alloy or intermetallic compound,[19] deposition of a metal oxide overlayer, using an organic modifier[20] or development of supports with defects or heteroatoms suitable for confining metals.[21] However, for Ni catalysts, deactivation as a result of carbonaceous deposits still significantly limits catalytic lifetime. As such, this has become a driving force for researchers to further develop alternative catalysts.

In this work, we report the use of a confinement strategy to fabricate a stable and atomically dispersed non-noble metal Ni catalyst (Ni_1MoS) on Al_2O_3 with Ni loading up to 3.5 wt. % for the selective hydrogenation of acetylene. Specifically, Mo_3S_4 clusters with a cubic structure cell allow a Ni atom to bond with S or Mo atoms on the cell edge and act as the crucial active site. Aberration-corrected electron microscopy and X-ray absorption spectroscopy are used to characterize the dispersion and chemical state of Ni species on the surface of alumina support. By virtue of combining these experiments with DFT calculations, a possible mechanism for selective C≡C hydrogenation is proposed.

2. Result and discussion

2.1 Synthesis and structural characterization of Ni_1MoS/Al_2O_3

A dark green $[Mo_3S_4(H_2O)_9]^{4+}$ metal cluster solution was first prepared by reacting ammonium tetrathiomolybdate with $NaBH_4$ and HCl.[22] The formation of this complex was confirmed by UV–visible spectroscopy (Fig. S1A). Nickel nitrate was then introduced into the metal cluster solution to allow the adsorption and bonding of Ni

(Fig. S1B). A supported catalyst was then prepared by a conventional impregnation route using Al_2O_3. The solid was washed thoroughly with water to remove chloride ions, and thermally pretreated/activated at 200°C in N_2 for 1 h as well as at 300°C in H_2 for 2 h (Fig. S2) to produce Ni_1MoS/Al_2O_3 catalyst. Except for the characteristics of the Al_2O_3 support, no obvious Ni nanoparticles are observed in STEM images at both low and high magnifications (Fig. 1A-D, Fig. S3 and S4). Similarly, XRD patterns (Fig. S5) of Ni_1MoS/Al_2O_3 catalyst before and after heat treatment (even with Ni loading as high as 3.5 wt. % Ni - determined by ICP-AES) showed no evidence of Ni or NiO nanoparticles. Furthermore, Energy Dispersive X-ray Spectroscopy (EDS) analysis was performed. The mapping images (Fig. 1C and S4) reveal that Ni, Mo and S are evenly dispersed on Al_2O_3 without any agglomerates observed. As a contrast, Ni free $[Mo_3S_4(H_2O)_9]^{4+}$ metal clusters were impregnated on Al_2O_3 to obtain a MoS/Al_2O_3 catalyst after the same thermal pre-treatment described above. This sample possesses Mo particles with the average size of 1.5±0.2 nm (observed by HRTEM) and a lattice spacing of 0.322 nm which is assigned to the (202) facet of the Mo_3S_4 phase (Fig. S6D and Table S1). The above results are also consistent with XRD analysis (Fig. S5). Characteristics for additional reference samples including Ni/Al_2O_3, NiS/Al_2O_3 and Mo/Al_2O_3 are shown in Fig. S6 and Table S1.

To gain more structural information on Ni_1MoS/Al_2O_3 catalyst, spherical aberration corrected HAADF-STEM was employed. The thermal pre-treatment removes H_2O (from the original metal cluster) to form Ni_1MoS/Al_2O_3 and subsequently allows direct observation for the separation of Ni atoms by Mo and S atoms on a sub nanometer scale by aberration-corrected STEM (see Fig. 1E-F and Fig. S7). That is to say, the Mo_3S_4 cluster provides a site for anchoring Ni from $Ni(NO_3)_2$ precursor, by forming Ni-S (Mo) bonds. We also used CO as an IR probe molecule (Fig. S8) to study the adsorption behavior and geometric states. Three bands are observed at 2100, 1637 and 1400 cm^{-1}. The band at 2100 cm^{-1} is attributed to CO adsorbed on oxidized Ni species in a top configuration,[23] while the other two bands correspond to formate and bicarbonate species formed from adsorbed CO interacting with Al-OH.[24] No signals associated with CO adsorbed on bridge or hollow sites are observed,[25] which serves as further evidence

of atomically dispersed Ni in the catalyst.

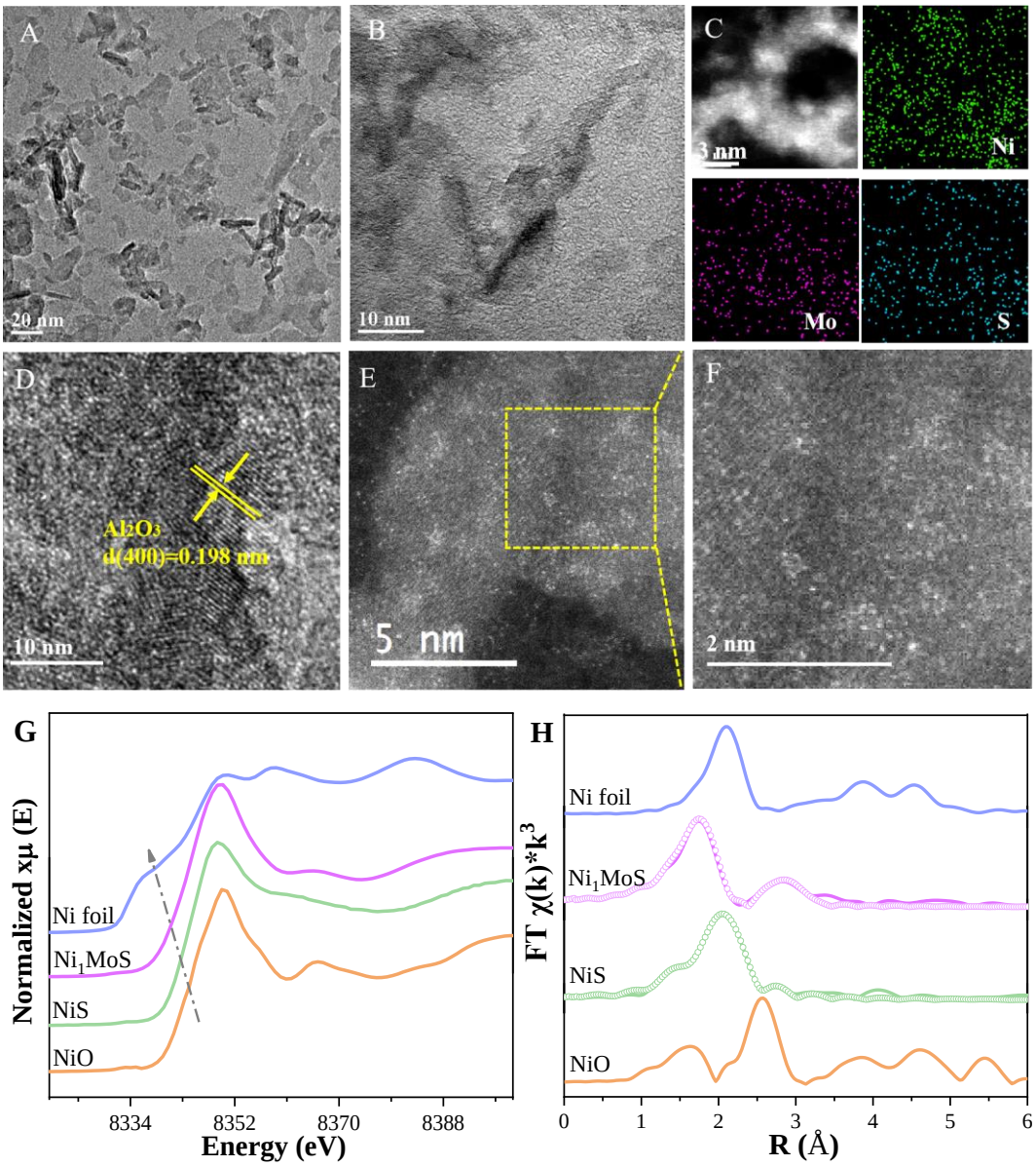

Fig. 1 Structural characterizations of Ni_1MoS/Al_2O_3. (A, B, D) Representative HRTEM images (C) STEM-EDS elemental mapping (E, F) AC-HAADF-STEM images of Ni_1MoS/Al_2O_3 catalyst (G) Normalized XANES spectra and (H) FT-EXAFS spectra of Ni K-edge EXAFS spectra for Ni_1MoS/Al_2O_3, NiS/Al_2O_3, NiO, and Ni foil.

Fig. 1G presents the X-ray Absorption Near-Edge Structure (XANES) spectra of Ni_1MoS/Al_2O_3 and NiS/Al_2O_3 materials (Ni foil and NiO spectra are included for reference). The near-edge lines in Ni_1MoS/Al_2O_3 and NiS/Al_2O_3 samples are similar to those of NiO reference but the former has somewhat lower energy. This indicates the

oxidation state of Ni atoms in Ni_1MoS/Al_2O_3 is positive.[26] These results are consistent with XPS analysis (Fig. S9), where the Ni $2p_{3/2}$ signal in Ni_1MoS/Al_2O_3 catalyst shifts to a lower energy of 856.0 eV compared with the peaks attributed to Ni^{2+} in the $[Mo_3NiS_4(H_2O)_{10}]^{4+}/Al_2O_3$ precursor and NiS/Al_2O_3 sample. In other words, both XANES and XPS suggest the Ni oxidation state in Ni_1MoS/Al_2O_3 is positive but below 2 (i.e., $Ni^{\delta+}$ species where δ lies in the range of 0-2).[27]

More structural information is provided by analyzing the Extended X-ray Absorption Fine Structure (EXAFS) at the Ni K-edge, as shown in Fig. 1H. A notable peak appears in the region of 1 to 2 Å in Ni_1MoS/Al_2O_3 but the intensity is significantly lower than that of the NiO reference, implying a distorted structure around the nearest coordination of Ni atoms. That is to say, the first shell peak for Ni_1MoS/Al_2O_3 is different from NiO and could be ascribed to a Ni-S contribution with a bond length of 2.17 Å.[28] More importantly and consistent with expectation, there is no peak originating from a Ni-Ni contribution.[29] An atomic distance of ca. 3.20 Å is apparent in Ni_1MoS/Al_2O_3 but not in NiS/Al_2O_3. As such, it may be indicative of a Ni-Mo interaction.[30] These results can be considered as clear evidence for the sole presence of dispersed Ni atoms in Ni_1MoS/Al_2O_3 precluding the existence of metallic Ni particles.[31] The local coordination numbers (CN) of the Ni-S first shell and Ni-Mo second shell in Ni_1MoS/Al_2O_3 were fitted as 2.7 and 1.7, respectively.[32] For NiS/Al_2O_3 sample, no obvious agglomeration is observed in STEM-mapping images, although a peak attributed to Ni-Ni coordination is observed in EXAFS along with a Ni-S coordination at 2.18 Å (Table S2). A fitted Ni-Ni distance of 2.51 Å and CN of 8.8 suggest the existence of Ni ensembles in this sample with small particle size but in quite low level since the Ni−Ni CN is far smaller than that in Ni foil (CN = 12).[32]

2.2 Evaluation of catalytic behavior

The selective hydrogenation of acetylene was chosen as a model reaction to evaluate the catalytic behavior of single Ni atoms in $NiMoS/Al_2O_3$, using Al_2O_3 supported Ni, NiS, Mo, MoS catalysts as reference materials. As displayed in Fig. 2A, the conversions of all catalysts increase with increasing reaction temperature. For Mo/Al_2O_3 and

MoS/Al_2O_3, no hydrogenation is observed at temperatures lower than 200°C, implying that Mo and MoS are largely inert (Fig. S10). The performance of Ni/Al_2O_3 catalyst is consistent with expectation – it exhibits complete acetylene conversion at 200°C but with alkene selectivity below 0. Two key points can be taken from the data presented. Firstly, Ni is considered as the catalytically active element. Secondly, this poor performance is associated with continuous Ni ensembles, which lead to the appearance of undesired ethane and green oil/oligomers. Interestingly, complete acetylene conversion and excellent ethylene selectivity (90% in Fig. 2B) are obtained over the Ni_1MoS/Al_2O_3 single atom catalyst at 125°C. The reaction temperature to achieve complete conversion for this catalyst is lower than that of either NiS/Al_2O_3 or Ni/Al_2O_3 samples. Similarly, the reaction rate, reflecting the intrinsic activity, of Ni_1MoS/Al_2O_3 is calculated as 0.094 mol^{-1} g_{cat}^{-1} s^{-1}, which exceeds that of NiS/Al_2O_3 and Ni/Al_2O_3. Meanwhile, the apparent activation energy (E_a) over Ni_1MoS/Al_2O_3 (derived from the linear fitting of ln(TOF) versus 1000/T - Fig. 2C) is similar with Ni/Al_2O_3, indicating that the site isolated Ni catalysts possess excellent catalytic activity. In terms of selectivity, NiS/Al_2O_3 catalyst shows good ethylene selectivity of 78% at full acetylene conversion, which may be related to decreased contiguous Ni sites. Indeed, this level of selectivity is similar to that reported for a bulk phase Ni_2S_3 sample.[33] Moreover, compared with reported non-noble metal catalysts (see Table S3), the site-isolated Ni_1MoS/Al_2O_3 could be considered as the most selective catalyst reported to date (ethylene selectivity of 90% at 100% conversion). These results indicate that the addition of Mo and S effectively isolates the Ni sites and thus promotes the selective conversion of acetylene into ethylene. Generally, spherical Al_2O_3 pellets are widely used in industry and thus the active Ni_1MoS component was further supported on spherical Al_2O_3 to obtain $Ni_1MoS/S\text{-}Al_2O_3$. As expected, this catalyst displays reasonable activity and selectivity, which provides the possibility for the substitution of precious metals in industry (although the activity and selectivity are lower than powder Al_2O_3 supported Ni catalysts due to the mass transfer resistance, meaning further optimization is necessary).

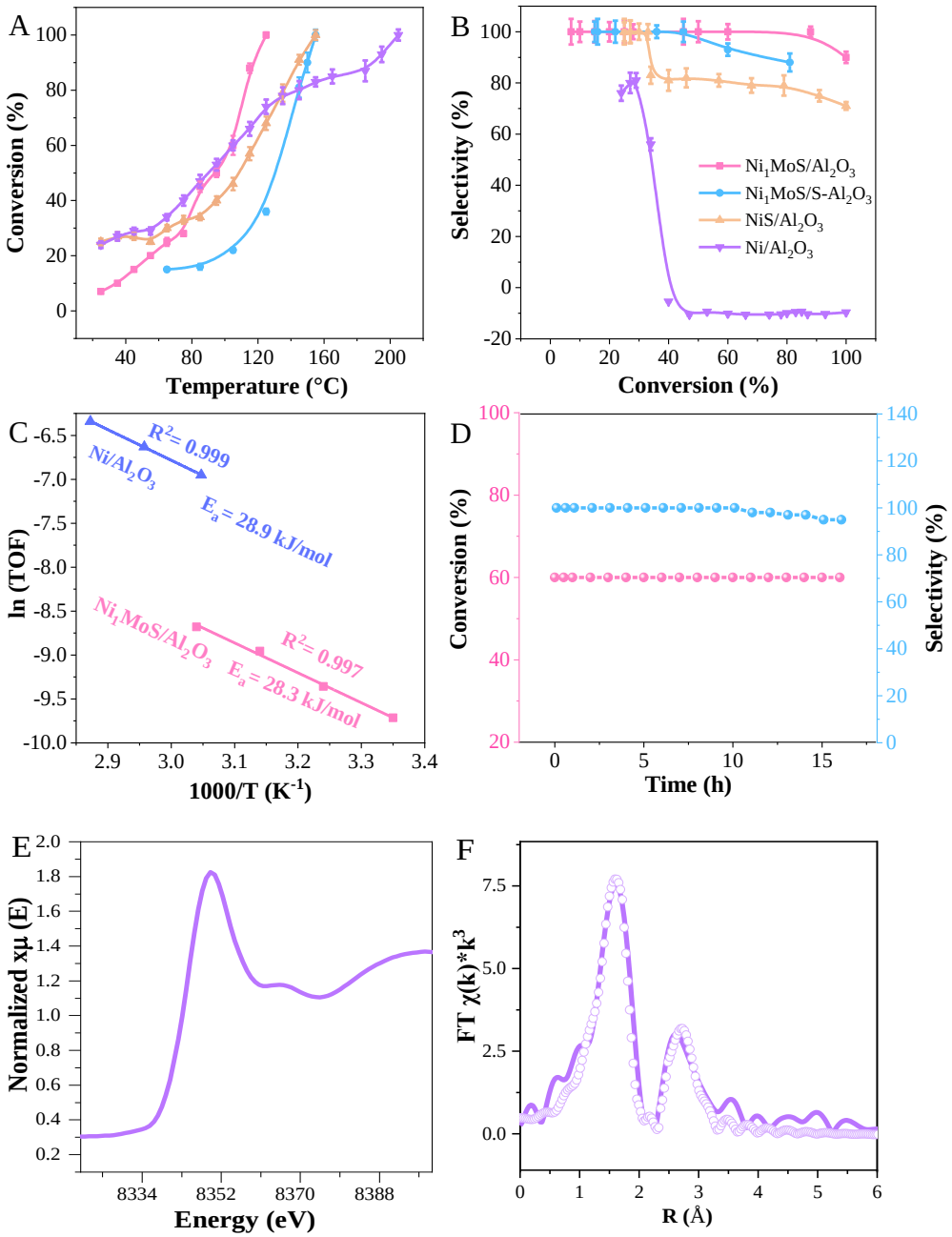

Fig. 2 Catalytic performance in the selective hydrogenation acetylene and characterizations of spent catalysts. (A) Acetylene conversion as a function of reaction temperature and (B) ethylene selectivity as a function of acetylene conversion over Ni-based catalysts ($Ni_1MoS/S\text{-}Al_2O_3$ stands for spherical Al_2O_3 supported Ni_1MoS). Error bars represent standard deviation from three independent measurements (Reaction conditions: 0.5 g of catalyst, 20:1 of H_2/C_2H_2 ratio, total flow = 165 mL min^{-1}, SV = 9900 h^{-1}). (C) Arrhenius plots of Ni_1MoS/Al_2O_3 and Ni/Al_2O_3 catalysts. (D) Long-term stability test for Ni_1MoS/Al_2O_3 at 105°C for 16 h. (E) Normalized Ni K-edge XANES and (F) EXAFS spectra for spent Ni_1MoS/Al_2O_3 and the corresponding fitting.

Importantly, the activity (Fig. 2D) is maintained with only a small decrease in ethylene selectivity over a 16 h testing period. Based on DFT calculations (Fig. S11), breaking of the Ni–S bonds (anchoring Ni atom through three S atoms) is endothermic by more than 4 eV (this phenomenon is in agreement with the report by Lu et al.[34]), which ensures the high chemical stability of this catalyst. Moreover, no Ni-Ni bonds at ca. 2.49 Å is observed in normalized XANES and EXAFS spectra for spent Ni_1MoS/Al_2O_3 (Fig. 2E and 2F), demonstrating that the atomically dispersed structure is robust under the catalytic conditions used. There is also no detectable oligomerization or Ni agglomeration after 16 h, assessed by TG-MS and STEM results, respectively, (Fig. S12 and S13). In contrast, a significant decrease in activity is observed for Ni/Al_2O_3 in only 3 h (Fig. S14). Since acetylene hydrogenation is a zero-order reaction (Fig. S15) the reaction rate is independent of the acetylene concentration,[35] meaning this decline in reaction rate of Ni/Al_2O_3 is caused by a change to the catalyst, namely sintering (Fig. S16) or more likely, carbonaceous deposits.

2.3 Probing the mechanism of selective acetylene hydrogenation.

The Ni atom introduced into the Mo_3S_4 cluster to form the site-isolated metal catalyst is responsible for the catalytic behavior; however, the exact function of these single Ni atoms remains unclear. To seek greater insight into the origins of the active sites, the reaction rates of Ni_1MoS/Al_2O_3 catalysts with various Ni contents were measured. It is found that with a progressive increase of Ni loading from 0.6% to 3.5%, the reaction rate of the catalyst increases linearly with Ni loading (Fig. 3A-B), while the selectivity remains unchanged (see Fig S17). This indicates that the method of introducing single Ni atoms into the Mo_3S_4 cluster is reasonably robust. However, when the Ni loading increases to 5%, the reaction rate and product selectivity decrease (Fig. 3A-B and Fig. S18). To explore this performance change, HRTEM analysis was performed and shows agglomerated Ni species with a particle size of 0.8±0.1 nm (Fig. S19). So why do the site-isolated Ni_1MoS catalysts possess far superior catalytic performance compared with a traditional supported Ni catalyst? It is generally accepted that H_2 undergoes

homolytic dissociation on the surface of nanosized metal catalysts (with more than two Ni atoms in the vicinity) into H atoms.[36] However, in this system, all Ni atoms in Mo_3S_4 cluster are individually dispersed, which is likely to give an alternative pathway for the dissociation of H_2.[37] To better understand why the Ni_1MoS/Al_2O_3 catalyst possesses such high catalytic activity, the energetics of hydrogen adsorption/activation were explored by DFT calculations (Fig. 3C). A H_2 molecule adsorbs on a Ni single atom with an adsorption energy of -0.65 eV and is readily heterolytically dissociated into two H atoms, one of which sits on the Ni atom and possesses a partial negative charge ($H^{\delta-}$), while the other H binds to a neighboring S atom.[38] The negatively charged $H^{\delta-}$ bound to the single Ni atom is less stable and is thus rapidly involved in hydrogenation catalysis. For comparison, a H_2 molecule on Ni ensembles is homolytically dissociated with adsorption energy of -0.58 eV as reported,[39] which indicates that the site-isolated Ni_1MoS catalyst provides a more active H species compared with monometallic Ni sample. This matches well with H_2-TPD analysis (Fig. S20), with greater desorbed amount of H_2 from site-isolated Ni catalyst than Ni/Al_2O_3.

Generally, the facile dissociation of reactants and weak binding of intermediates are key requirements for efficient and selective catalysis. These two variables are intimately linked in a way that does not generally allow the optimization of both properties simultaneously. However, with isolated Ni atoms dispersed in MoS nanoparticles, both preferable selectivity and high activity can be simultaneously achieved. To gain greater insight into why this is, in-situ DRIFTS experiments on Ni_1MoS/Al_2O_3, NiS/Al_2O_3 and Ni/Al_2O_3 catalysts were performed (Fig. 3D-F and S21). Since the molecular structures of ethylene and acetylene are symmetrical, there is no change in dipole moment, and thus the absorption peaks of C=C and C≡C cannot be detected in the infrared spectrum. As a result, propyne was employed as the reactant to simulate the selective hydrogenation of acetylene at different reaction temperatures.

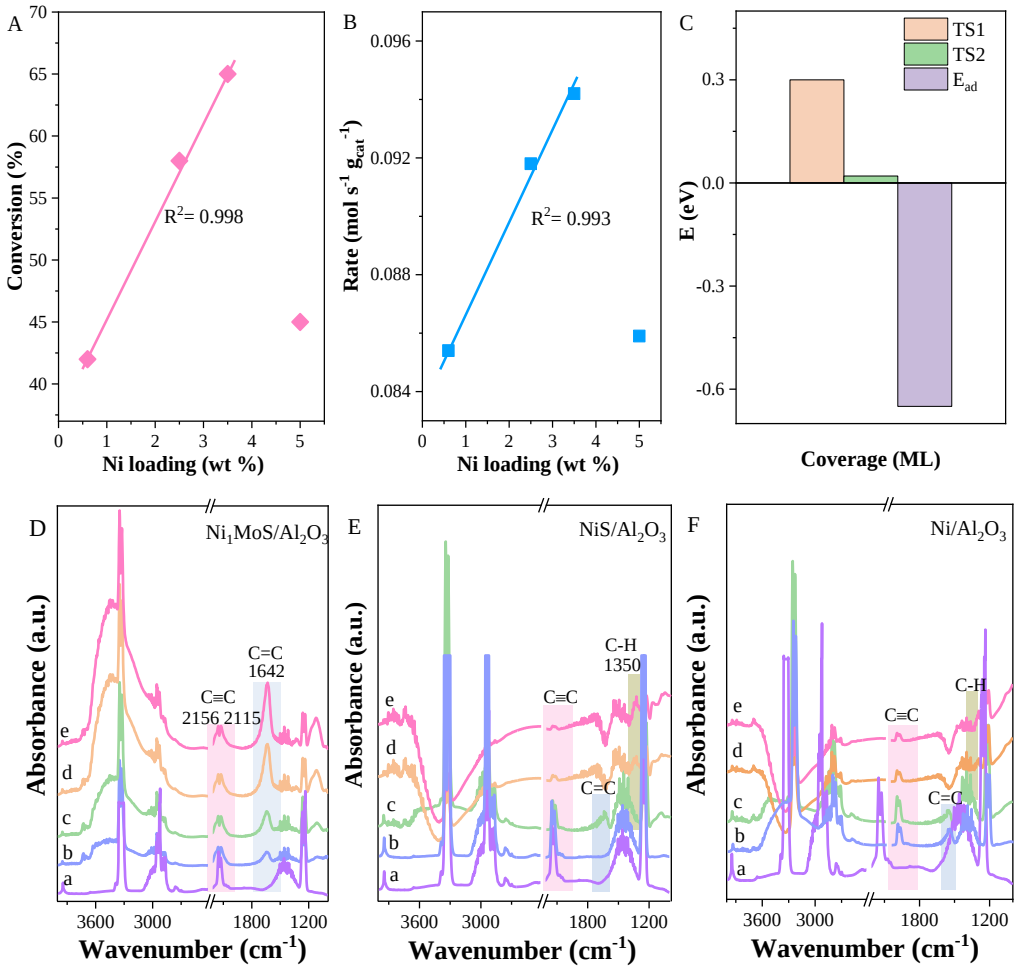

Fig. 3 Identification of active sites and the interaction with reactants. (A) The initial activities and (B) reaction rate as a function of the Ni loading (0.6, 2.5, 3.5 and 5.0 wt. %) for Ni_1MoS/Al_2O_3. The excellent linear correlation between the initial activity and Ni concentration supports the formation of isolated Ni sites. (C) The adsorption energy of H_2 molecule (E_{ad}) and the energy for C_2H_2* hydrogenation to C_2H_3* intermediate (TS1) and C_2H_3* hydrogenation to C_2H_4* intermediate (TS2) on Ni_1MoS/Al_2O_3. (D-F) In situ DRIFT spectra with the reactants of Ni_1MoS/Al_2O_3, NiS/Al_2O_3 and Ni/Al_2O_3. The spectra were obtained after (a) exposed in pure C_3H_4 (b) further introduced H_2, heating at (c) 60°C, (d) 100°C, (e) 120°C for 0.5 h for desorption.

Intense bands in the regions of 3300-3360, 2115-2156 and 2920-2980 cm^{-1} are observed in the infrared spectrum of Ni_1MoS/Al_2O_3 catalysts, attributed to unsaturated C-H and C-C vibrations (H-C≡C), as well as saturated C-H vibrations in propyne (-CH_3).[40] With the introduction of 10% H_2/N_2, the band intensity in the range of 3300–3360 cm^{-1} reduces rapidly, while two obvious bands appear at 1642 and 1121 cm^{-1}

corresponding to C=C and C-H vibrations in H-C=C, consistent with conversion of the alkyne to alkene.[41] In contrast, the intensities of peaks in the regions of 3300-3360 and 2115-2156 cm^{-1} for NiS/Al_2O_3 and Ni/Al_2O_3 decrease gradually with prolonged reaction time and/or higher temperature. Interestingly, when the reaction temperature is below 60°C, a weak band characteristic of C=C can be observed at 1642 cm^{-1}, indicating the alkene is produced, but this disappears as temperature increases to 100°C. Meanwhile, a new characteristic shoulder appears at 1350 cm^{-1}, which belongs to the bending vibration peak of C-H in propane,[42] indicating that these catalysts mainly form propane. These above phenomena are consistent with the catalytic evaluation. According to reported literature,[43, 44] with respect to di-σ adsorption at continuous sites, C≡C bond is able to adsorb on isolated atoms in π-bound configuration to form a vinyl species, which is easily hydrogenated to produce the ethylene with low desorption energy.

Furthermore, detailed DFT calculations have been performed according to the structure model (the corresponding CIF file is shown in the Supporting Information), in which the electronic state and local coordination are basically consistent with experimental results, confirmed by atomic bonding and Bader charge analysis (Fig. S22). The reaction energies of elementary steps are shown in Fig. 4. C_2H_2 coordinates easily on isolated Ni atom in a π-complex manner with an adsorption energy of -1.47 eV. The resulting C_2H_2* species is hydrogenated in two successive steps to produce C_2H_3*-Ni intermediate and then C_2H_4*-Ni species with barriers of only 0.30 eV (TS1) and 0.02 eV (TS2), displayed in Fig. 3C. These barriers are far lower than values reported for catalysts with larger Ni ensembles,[45] which further reveals why the Ni_1MoS/Al_2O_3 catalyst is highly active for acetylene hydrogenation.

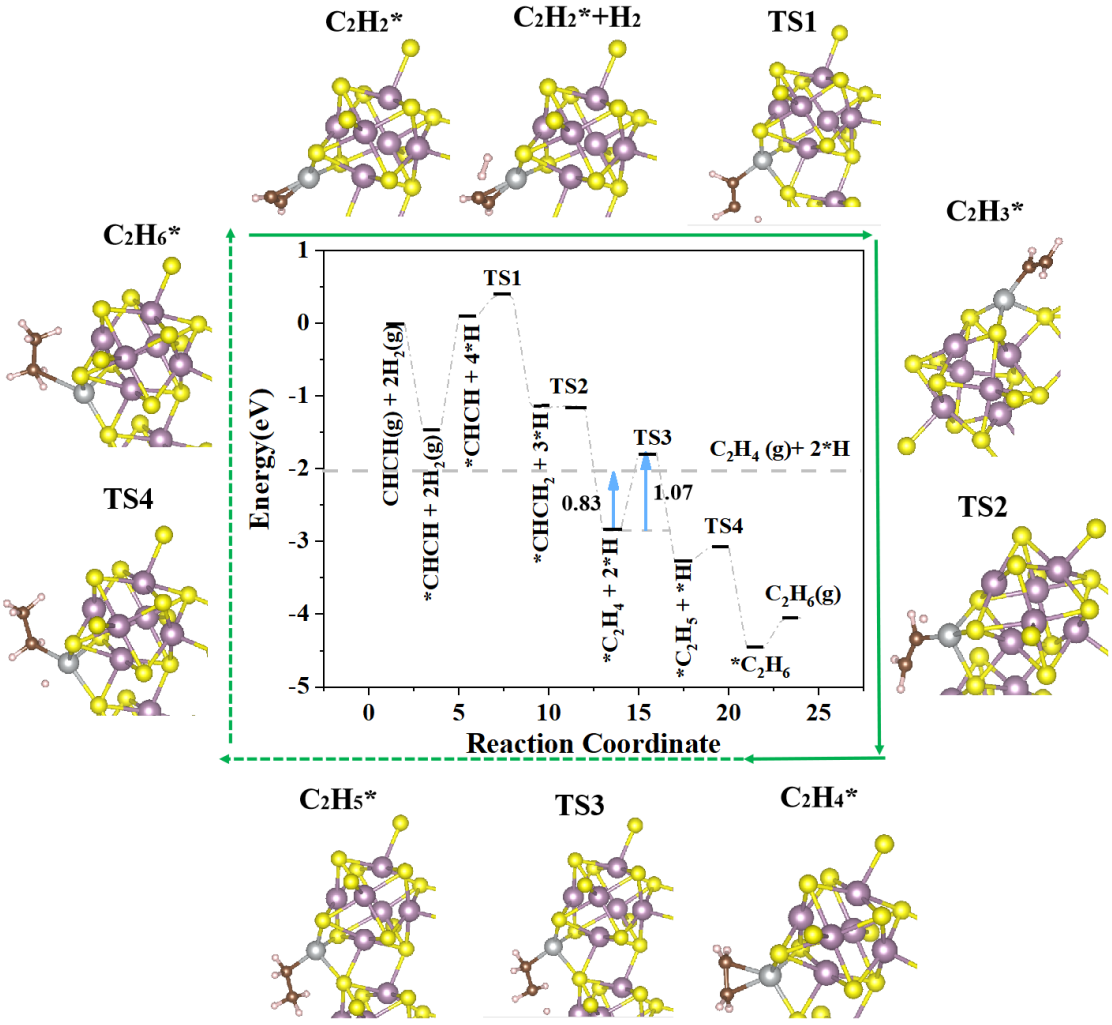

Fig. 4 DFT calculation optimized reaction path in acetylene hydrogenation for Ni_1MoS/Al_2O_3. The green arrows point out the reaction direction, where the solid line stands for the main reaction and the dotted line stands for the side reaction. The first and second blue arrows highlight the desorption of C_2H_4* to form C_2H_4 (g) and hydrogenation to the transition state, respectively.

The adsorption energy of obtained C_2H_4 species is -0.83 eV. As theoretically reported in a previous study,[46] the selectivity can be described by the difference between the ethylene desorption barrier and its subsequent hydrogenation barrier. In our system, the elementary step for ethylene over-hydrogenation to generate C_2H_5* is still thermodynamically feasible on isolated Ni active sites but with a barrier of 1.07 eV, much higher than the energy of ethylene desorption. The calculation demonstrates ethylene desorption is more favorable on single Ni atoms, consistent with the

experimental evidence derived from C_2H_4-TPD analysis (Fig. S23). However, in terms of the Ni ensembles, acetylene is adsorbed in the 3-fold coordinated hollow site on a Ni trimer with energy of -2.52 eV, leading to the production of C_2H_4* adsorbed in a di-σ configuration with the energy of −0.57 eV.[47] This energy is a little lower than the over-hydrogenation barrier, contributing to relatively low ethylene selectivity. The results described here are in line with the pioneering work concerning C_2H_2 hydrogenation over single metal atoms.[48]

Obviously, the confinement route from the cubic structure cell offers an opportunity to obtain stable Ni single atom catalysts. To explore this further, the exothermic rate of Ni single atom and ensembles as a function of the reaction temperature is given in equation 1:

$$Q_{site} = \frac{CF}{m \times w \times D} \Delta H \qquad \text{equation 1}$$

where Q_{site} means distributing the overall heat to the single active sites, C and F stand for the conversion and flow rate of C_2H_2, ΔH is the enthalpy change for the hydrogenation of acetylene, m, *w and D* are the catalyst quantity, metal loading and dispersion, respectively. As displayed in Fig. S24, the Q_{site} value displays the trend of Ni_1MoS/Al_2O_3 < Ni/Al_2O_3. Smaller Q_{site} value of Ni_1MoS/Al_2O_3 is positively related to higher metal dispersion, contributing to an increase in the number of the reaction sites and accordingly decreases the effective heat generation on each active site. This prevents accumulation of reaction heat on a specific active site and thereby inhibits the agglomeration of active components. The maintaining of Ni single atom structure in turn suppresses the generation of green oil/oligomers to some extent. In contrast, the heat generation is greater by a factor of 10 on Ni ensembles, indicating that a large amount of heat will accumulate on Ni nanoparticle catalyst and promote aggregation and coking.

In summary, we have reported a new strategy to fabricate a stable and site-isolated non-noble metal Ni_1MoS catalyst on Al_2O_3 by effectively confining isolated Ni atoms within the cubic structure cell of a Mo_3S_4 cluster. Site-isolated catalyst with Ni loading up to 3.5 wt. % can be prepared without any apparent Ni agglomeration. HAADF-

STEM and XAFS both confirmed the presence of isolated Ni atoms, which bonded with Mo and S atoms to create a new active site. By evaluating performance in the selective hydrogenation of acetylene, the Ni_1MoS/Al_2O_3 catalyst with isolated Ni sites exhibited 90% ethylene selectivity at a conversion of 100% under a relatively mild reaction temperature of 125°C, which far exceeded that of catalysts with contiguous Ni ensembles. More importantly, excellent long-term stability was obtained with no deactivation via either Ni atom aggregation or coking during a 16 h time on stream. The unique Ni single atom site favoured heterolytic activation of H_2 to yield a reactive $H^{\delta-}$ species, which enabled a good hydrogenation rate of unsaturated C≡C bonds. Through the use of in-situ DRIFTS studies and computational modeling with density functional theory, a π-adsorption mode of acetylene on isolated Ni atoms as well as an electronic effect induced by Mo and S play important roles in the improvement of ethylene selectivity. As such, the Ni_1MoS/Al_2O_3 catalyst represents a marked step forward in the design of hydrogenation catalysts.

ASSOCIATED CONTENT

Supporting Information

The supporting information is available free of charge at https://pubs.acs.org/doi.

This includes details of experiments; UV-vis spectra of precursors; STEM images, CO-IR, XPS, TG-MS and H_2-TPD results of fresh and spent Ni-based catalysts; XRD patterns of Al_2O_3 support and Ni-based catalysts; Comparison of catalytic performance over Ni-based catalysts; The exothermic rate on single active site at different reaction temperatures.

Author Contributions

B. Fu carried out most of the characterization, structural analysis as well as the catalytic reactions. Y. Liu conceived and designed the experiment, carried out the DFT calculations. S. Weng, Y. Song and J. Feng synthesized the experimental samples, while D. Li and Y. He provided the fund supporting. Y. Liu and A.J. McCue discussed the results and wrote the manuscript.

Notes

The authors declare no competing financial interest.

ACKNOWLEDGMENTS

This work was financially supported by National Natural Science Foundation of China (21908002) and the Fundamental Research Funds for the Central Universities (buctrc201921, JD2108).

References

(1) Ji, S. F.; Chen, Y. J.; Wang, X. L.; Zhang, Z. D.; Wang, D. S.; Li, Y. D. Chemical Synthesis of Single Atomic Site Catalysts. *Chem. Rev.* **2020,** *120,* 11900-11955.

(2) Zhao, Z. J.; Liu, S. H.; Zha, S. J.; Cheng, D. F.; Studt, F.; Henkelman, G.; Gong, J. L. Theory-Guided Design of Catalytic Materials using Scaling Relationships and Reactivity Descriptors. *Nat Rev Mater.* **2019,** *4,* 792-804.

(3) Ledendecker, M.; Pizzutilo, E.; Malta, G.; Fortunato, G. V.; Mayrhofer, K. J. J.; Hutchings G. J.; Freakley, S. J. Isolated Pd Sites as Selective Catalysts for Electrochemical and Direct Hydrogen Peroxide Synthesis. *ACS Catal.* **2020,** *10,* 5928-5938.

(4) Liu, Y. W.; Wang, B. X.; Fu, Q.; Liu, W.; Wang, Y.; Gu, L.; Wang, D. S.; Li, Y. D. Polyoxometalate-Based Metal-Organic Framework as Molecular Sieve for High Selective Semi-hydrogenation of Acetylene on Isolated Single Pd Atom Site. *Angew. Chem. Int. Ed.* **2021**, *60,* 22522-22528.

(5) Zhang, Q.; Qin, X. X.; Duan-Mu, P. F.; Ji, H. M.; Shen, Z. R.; Han, X. P.; Hu, W. B. Isolated Platinum Atoms Stabilized by Amorphous Tungstenic Acid: Metal–Support Interaction for Synergistic Oxygen Activation. Angew. *Chem. Int. Ed.* **2018,** *57,* 9351-9356.

(6) Chen,Y. J.; Ji, S. F.; Chen, C.; Peng, Q.; Wang, D. S.; Li, Y. D. Single-Atom Catalysts: Synthetic Strategies and Electrochemical Applications. *Joule.* **2018,** *2,* 1242-1264.

(7) Han, A.; Zhang, Z. D.; Yang, J. R.; Wang, D. S.; Li, Y. D. Carbon-Supported Single-Atom Catalysts for Formic Acid Oxidation and Oxygen Reduction Reactions. *Small.* **2021,** *17,* 2004500.

(8) Yan, D. X.; Chen, J.; Jia, H. P. Temperature-Induced Structure Reconstruction to Prepare a Thermally Stable Single-Atom Platinum Catalyst. *Angew. Chem. Int. Ed.* **2020,** *59,* 13562-13567.

(9) Ji, Z.; Trickett, C.; Pei, X. K.; Yaghi, O. M. Linking Molybdenum−Sulfur Clusters for Electrocatalytic Hydrogen Evolution. *J. Am. Chem. Soc.* **2018,** *140,* 13618-13622.

(10) Qin,Y. Y.; Wu, L.; Li, Z.J.; Kang, Y.; Tang,Y. H.; Yao, Y. G. A Sandwich Cubane-Type Mo–Sn Cluster: Synthesis and Crystal Structure of $[(H_2O)_9Mo_3OS_3SnS_3OMo_3(H_2O)_9](CH_3C_6H_4SO_3)_8\cdot 18H_2O$. *Chemi. Lett.* **2000,** *29,* 950-951.

(11) Qin, Y. Y.; Li, Z. J.; Kang, Y.; Zhang, J.; Yao, Y. G. Synthesis and Crystal Structure of a Mo-S

Cluster Compound Coordinated by Isonicotinate. *Chinese J Struc Chem.* **2007,** *26,* 1043-1046.
(12) Jiang, J.; Gao, M. R.; Sheng, W. C.; Yan, Y. S. Hollow Chevrel-Phase $NiMo_3S_4$ for Hydrogen Evolution in Alkaline Electrolytes. *Angew. Chem. Int. Ed.* **2016,** *55,* 15240-15245.
(13) McCue, A. J.; Guerrero-Ruiz, A.; Ramirez-Barria, C. Rodríguez-Ramos, I.; Anderson, J. A. Selective Hydrogenation of Mixed Alkyne/Alkene Streams at Elevated Pressure over a Palladium Sulfide Catalyst. *J. Catal.* **2017,** *355,* 40-52.
(14) Kojima, T.; Kameoka, S.; Fujii, S.; Ueda, S.; Tsai, A.P. Catalysis-Tunable Heusler Alloys in Selective Hydrogenation of Alkynes: A New Potential for Old Materials. *Sci. Adv.* **2018,** *4,* 6063-6070.
(15) Yan, H.; Cheng, H.; Yi, H.; Lin, Y.; Yao, T.; Wang, C. L.; Li, J. L.; Wei, S. Q.; Lu, J. L. Single-Atom Pd_1/Graphene Catalyst Achieved by Atomic Layer Deposition: Remarkable Performance in Selective Hydrogenation of 1,3-Butadiene. *J. Am. Chem. Soc.* **2015,** *137,* 10484-10487.
(16) Albani, D.; Shahrokhi, M.; Chen, Z.; Sharon Mitchell.; Hauert, R.; López, N.; Pérez-Ramírez, J. Selective Ensembles in Supported Palladium Sulfide Nanoparticles for Alkyne Semi-Hydrogenation. *Nat Commun.* **2018,** *9,* 2634.
(17) Albani, D.; Karajovic, K.; Tata, B.; Li, Q.; Mitchell, S.; López, N.; Pérez-Ramírez, J. Ensemble Design in Nickel Phosphide Catalysts for Alkyne Semi-Hydrogenation. *ChemCatChem.* **2019,** *11,* 457-464.
(18) Spanjers, C. S.; Sim, R. S.; Sturgis, N. P.; Kabius, B.; Rioux, R. M. In Situ Spectroscopic Characterization of Ni_xZn_{1-x}/ZnO Catalysts and Their Selectivity for Acetylene Semi-Hydrogenation in Excess Ethylene. *ACS Catal.* **2015,** *5,* 3304-3315.
(19) Ferrando, R.; Jellinek, J.; Johnston, R. L.; Nanoalloys: From Theory to Applications of Alloy Clusters and Nanoparticles. *Chem. Rev.* **2008,** *108,* 845–910.
(20) Norskov, J. K.; Bligaard, T.; Rossmeisl, J.; Christensen, C. H. Towards the Computational Design of Solid Catalysts. *Nat. Chem.* **2009,** *1,* 37-46.
(21) Zhang, L. L.; Zhou, M. X.; Wang, A. Q; and Zhang, T. Selective Hydrogenation over Supported Metal Catalysts: From Nanoparticles to Single Atoms. *Chem. Rev.* **2020,** *120,* 683–733.
(22) Shibahara, T.; Yamasaki, M.; Sakane, G.; Minami, K.; Yabuki, T.; Ichimura1, A. Syntheses and Electrochemistry of Incomplete Cubane-Type Clusters with M_3S_4 Cores (M = Mo, W). X-ray Structures of $[W_3S_4(H_20)_9]$ $(CH_3C_6H_4SO_3)_4{\cdot}9H_2O$, $Na_2[W_3S_4(Hnta)_3]{\cdot}5H_2O$, and $(bpyH)_5[W_3S_4(NCS)_9]{\cdot}3H_2O$. *Inorg. Chem.* **1992,** *31,* 640-647.
(23) Cao, Z. K.; Zhang, X.; Guo, R.; Ding, S. J.; Zheng, P.; Fan, J. Y.; Mei, J. L.; Xu, C. M.; Duan. A. Synergistic Effect of Acidity and Active Phases for NiMo Catalysts on Dibenzothiophene Hydrodesulfurization Performance. *Chem. Eng. J.* **2020,** *400,* 125886.
(24) Ni, J.; Leng, W.; Mao, H. J.; Wang, J. G.; Lin, J. Y.; Jiang, D. H.; Li, X. N. Tuning Electron Density of Metal Nickel by Support Defects in Ni/ZrO_2 for Selective Hydrogenation of Fatty Acids to Alkanes and Alcohols. *Appl. Catal. B.* **2019,** *253,* 170-178.
(25) Zacharaki, E.; Beato, P.; Tiruvalam, R. R.; Andersson, K. J.; Fjellvag, H.; Sjastad, A. O. From

Colloidal Monodisperse Nickel Nanoparticles to Well-Defined Ni/Al_2O_3 Model Catalysts. *Langmuir.* **2017,** *33,* 9836-9843.

(26) Chai, Y. C.; Wu, G. J.; Liu, X. Y.; Ren, Y. J.; Dai, W. L.; Wang, C. M.; Xie, Z. K.; Guan, N. J.; Li, L. D. Acetylene-Selective Hydrogenation Catalyzed by Cationic Nickel Confined in Zeolite. *J. Am. Chem. Soc.* **2019,** 141, 9920-9927.

(27) Zhou, Y. X.; Luo, M.; Zhang, W.; Zhang, Z. X.; Meng, X. D.; Shen, X. S.; Liu, H. F.; Zhou, M.; Zeng, X.H. Design and Synthesis of Highly Performing Bifunctional Ni-NiOMoNi Hybrid Catalysts for Enhanced Urea Oxidation and Hydrogen Evolution Reactions. *ACS Sustainable Chem. Eng.* **2020,** *8,* 7174-7181.

(28) Ma, Q.Y.; Hua, C.Y.; Liu, K. L.; Hung, S. Fu.; Ou, D. H.; Chen, H. M.; Fu, G.; Zheng, N. F. Identifying the Electrocatalytic Sites of Nickel Disulfide in Alkaline Hydrogen Evolution Reaction. *Nano Energy*. **2017,** *41,* 148-153.

(29**)** Yin, J.; Jin, J.; Zhang, H.; Lu, M.; Peng, Y.; Huang, B. L.; Xi, P. X.; Yan, C. H. Atomic Arrangement in Metal-Doped NiS_2 Boosts the Hydrogen Evolution Reaction in Alkaline Media. *Angew. Chem. Int. Ed.* **2019,** *58,* 18676-18682.

(30) Gaur, A.; Dabros, T. M. H.; Høj, M.; Boubnov, A.; Prüssmann, T.; Jelic, J.; Studt, F.; Jensen, A. D.; Grunwaldt, J. D. Probing the Active Sites of MoS_2 Based Hydrotreating Catalysts Using Modulation Excitation Spectroscopy. *ACS Catal.* **2019,** *9,* 2568-2579.

(31) Taniguchi, M.; Imamura, D.; Ishige, H.; Ishii, Y.; Murata, T.; Hidai, M.; Tatsumi, T. Hydrodesulfurization of Benzothiophene over Zeolite-Supported Catalysts Prepared from Mo and Mo–Ni Sulfide Clusters. *J. Catal.* **1999,** *187,* 139-150.

(32) Pattengale, B.; Huang, Y. C.; Yan, X. X.; Yang, S. Z.; Younan, S.; Hu, W. H.; Li, Z. D.; Lee, S.; Pan, X. Q.; Gu, J.; Huang, J. Dynamic Evolution and Reversibility of Single-Atom Ni (II) Active Site in 1T-MoS_2 Electrocatalysts for Hydrogen Evolution. *Nat Commun.* **2020,** *11,* 4114.

(33) McCue, A. J.; Guerrero-Ruiz, A.; Rodríguez-Ramos, I.; Anderson, J. A. Palladium Sulphide - A highly Selective Catalyst for the Gas Phase Hydrogenation of Alkynes to Alkenes. *J. Catal.* **2016,** *340,* 10-16.

(34) Gu, J.; Jian, M. Z.; Huang, L.; Sun, Z. H.; Li, A. W.; Pan, Y.; Yang, J. Z.; Wen, W.; Zhou, W.; Lin, Y.; Wang, H. J.; Liu, X. Y.; Wang, L. L.; Shi, X. X.; Huang, X. H.; Gao, L. N.; Chen, S.; Zheng, X. S.; Pan, H. B.; Zhu, J. F.; Wei, S. Q.; Li, W. X.; Lu, J. L. Synergizing Metal–Support Interactions and Spatial Confinement Boosts Dynamics of Atomic Nickel for Hydrogenations. *Nat. Nanotechnol.* **2021,** *16,* 1141–1149.

(35) Kiralya, Z.; Veiszb, B.; Mastalir. A. CS_2 Poisoning of Size-Selective Cubooctahedral Pd Particles in Styrene Hydrogenation. *Catal Lett.* **2004,** *95,* 57-59.

(36) Zhou, Y. N.; Sun, W. J.; Chu, W.; Zheng, J.; Gao, X. P.; Zhou, X.; Xue, Ying. Adsorption of acetylene on ordered Ni_xAg_{1-x}/Ni (111) and effect of Ag-dopant: A DFT study. *Appl. Surf. Sci.* **2018,** *435,* 521–528.

(37) Liu, W. G.; Chen, Y. G.; Qi, H. F.; Zhang, L. L.; Yan, W. S.; Liu, X. Y.; Yang, X. F.; Miao, S.;

Wang, W. T.; Liu, C. G.; Wang, A. Q.; Li, J.; Zhang, T. A Durable Nickel Single-Atom Catalyst for Hydrogenation Reactions and Cellulose Valorization under Harsh Conditions. *Angew.Chem. Int. Ed.* **2018,** *57,* 7071-7075.

(38) Kuai, L.; Chen, Z.; Liu, S. J.; Kan, E.; Yu, N.; Ren, Y. M.; Fang, C. H.; Li, X. Y.; Li, Y.D.; Geng, B. Y. Titania Supported Synergistic Palladium Single Atoms and Nanoparticles for Room Temperature Ketone and Aldehydes Hydrogenation. *Nat Commun.* **2020,** *11,* 48.

(39) Yang, B.; Burch, R.; Hardacre, C.; Headdock, G.; Hu, P. Origin of the Increase of Activity and Selectivity of Nickel Doped by Au, Ag, and Cu for Acetylene Hydrogenation. *ACS Catal.* **2012,** *2,* 1027-1032.

(40) Chu, M. Y.; Pan, Q.; Bian, W. Y.; Liu, Y.; Cao, M. H.; Zhang, C. Y.; Lin, H. P.; Zhang, Q.; Xu, Y. Strong Metal–Support Interaction Between Palladium and Gallium Oxide Within Monodisperse Nanoparticles: Self-Supported Catalysts for Propyne Semi-Hydrogenation. *J. Cata.* **2021,** *395,* 36-45.

(41) Jackson, S. D.; Casey, N. J.; Hydrogenation of Propyne Ouer Palladium Catalysts. *J. Chem. Soc. Faraday Trans*. **1995**, *91,* 3269-3274.

(42) Abdel-Rahman, M, K.; Trenary, M. Propyne Hydrogenation over a Pd/Cu(111) Single-Atom Alloy Studied Using Ambient Pressure Infrared Spectroscopy. *ACS Catal.* **2020**, *10,* 9716-9724.

(43) Hu, C. Q.; Sun, J. H.; Yang, Y. F.; Zhu, Q. S.; Yu, B. Reaction Pathway for Partial Hydrogenation of 1,3-Butadiene over Pt/SiO_2. *Catal. Sci. Technol*. **2017**, *7*, 5932-5943.

(44) Bridier, B.; López, N.; Pérez-Ramírez, J. Partial Hydrogenation of Propyne over Copper-Based Catalysts and Comparison with Nickel-Based Analogues. *J. Catal.* **2010**, *269,* 80-92.

(45) Rao, D. M.; Zhang, S. T.; Li, C. M.; Chen, Y. D.; Pu, M.; Yan, H.; Wei, M. The Reaction Mechanism and Selectivity of Acetylene Hydrogenation over Ni–Ga Intermetallic Compound Catalysts: A Density Functional Theory Study. *Dalton Trans.* **2018,** *47,* 4198-4208.

(46) Huang, F.; Deng, Y. C.; Chen, Y. L.; Cai, X. B.; Peng, M.; Jia, Z. M.; Xie, J. L.; Xiao, D. Q.; Wen, X. D.; Wang, N.; Jiang, Z.; Liu, H. Y.; Ma, D. Anchoring Cu_1 Species over Nanodiamond-Graphene for Semi-Hydrogenation of Acetylene. *Nat Commun.* **2019,** *10,* 4431.

(47) Jian, M. Z.; Liu, J. X.; Li, W. X. Hydroxyl Improving the Activity, Selectivity and Stability of Supported Ni Single Atoms for Selective Semi-Hydrogenation. *Chem. Sci.* **2021,** *12,* 10290.

(48) Huang, Fei.; Deng, Y. C.; Chen, Y. L.; Cai, X. B.; Peng, M.; Jia, Z. M.; Ren, P. J.; Xiao, D. Q.; Wen, X. D.; Wang, N.; Liu, H. Y.; Ma, D. Atomically Dispersed Pd on Nanodiamond/Graphene Hybrid for Selective Hydrogenation of Acetylene. *J. Am. Chem. Soc.* **2018,** *140,* 13142-13146.

Graphical abstract

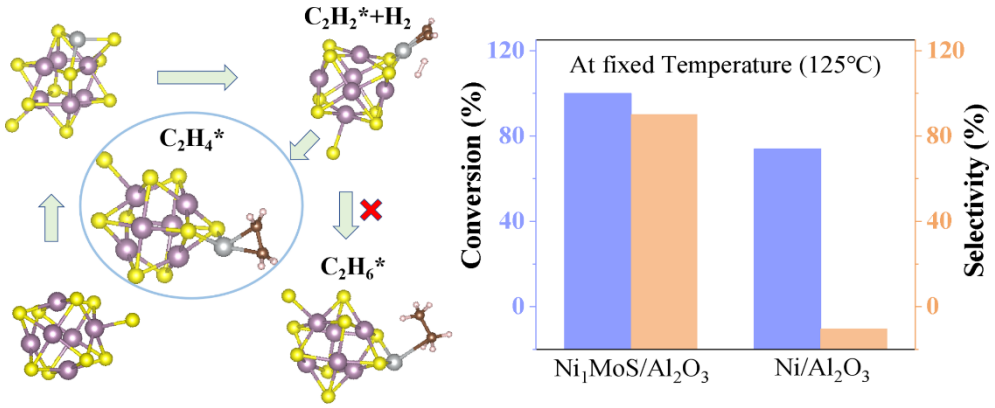
C2H2*+H2
C2H4*
C2H6*
At fixed Temperature (125°C)
Conversion (%)
Selectivity (%)
120
80
40
0
Ni1MoS/Al2O3
Ni/Al2O3